A Hardware-in-the-Loop Testbed for Microgrid Protection Considering Non-standard Curves

P. H. A. Barra, V. A. Lacerda, R. A. S. Fernandes, D. V. Coury

***Abstract*—This paper presents a hardware-in-the-loop testbed for microgrid protection, primarily intended for real-time testing of non-standard protection curves. Since these curves differ from those available in commercial relays, it is imperative to test their performance in a hardware environment. The protection curves and digital relay logic were embedded in four Texas Instruments C2000 Delfino F28379D Microcontroller unit (MCU) Launchpad tools, representing four relays within the microgrid. The real-time digital simulator (RTDS) was used to inject the analog signals into the MCUs. Fault conditions were used to compare the performance of the standard curves and non-standard ones. The obtained results showed that hardware implementation was successful due to their proximity to the simulation results. Real-time experiments reinforced the feasibility of the non-standard curves for protecting microgrids.**

***Keywords*—Hardware-in-the-Loop; Microgrid; Protection; Real-Time Simulator; Testbed.**

I. Introduction

THE share of renewable energy resources in the power sector continues to grow, which occurs not only in bulk transmission systems but also in distribution systems [1]. High penetration of these distributed energy resources (DERs) helps decarbonization of electric power systems and derives other benefits, such as reducing energy dependence on fossil fuels. However, there are some challenges for controlling and operating DER-intensive modern systems. The so-called microgrids partially fulfill the challenges associated with integrating multiple DERs, lines, and loads [2].

Microgrids can be defined as independent power networks that use local, distributed energy resources to provide grid backup or off-grid power to meet local needs. One key benefit of microgrids is their capacity to operate isolated from the main grid, called the islanded operation mode. Thus, if an abnormal event occurs in the main grid, the microgrid can be disconnected without interrupting the islanded loads' energy supply. This flexible operation is a reason why some authors point out that microgrids can improve efficiency, reliability, and overall system power quality [2]–[4].

Despite intrinsic advantages of microgrids, some technical challenges still exist, and among them, protection stands out [5]. Some challenges for protecting microgrids, when compared to the traditional distribution networks, can be highlighted: i) depending on the microgrid operation mode (islanded or connected), fault currents can vary substantially; ii) a bidirectional power flow naturally exists; iii) the microgrid topology can change for self-healing purposes; iv) some distributed energy resources are intermittent. These challenges have drawn much attention from the research community and industry, which are currently investigating new solutions and strategies to obtain reliable microgrid protection in relation to these and other difficulties.

Regarding this matter, [6] presented an extensive survey associated with protecting microgrids and distribution systems using distributed generators. This review discussed different adaptive protection strategies, including computational intelligence-based approaches. From this review, the predominance of using standard overcurrent-based protection among the discussed strategies should be highlighted. Papers that use standard protection functions usually combine directional overcurrent relays with adaptive protection strategies, such as [7]–[9]. Nevertheless, even with these recent papers' outcomes, the review presented in [6] highlighted the need for further efforts to obtain new strategies and solutions for microgrid protection.

Alternatively, new proposals can be found in the technical literature concerning non-standard characteristics for power system protection, i.e., characteristics not seen in the current standards. These new solutions aim to address the challenges of modern power systems and are possible due to the large utilization of digital relays. In this context, [10] presented a review of recent research that proposed non-standard characteristics. Moreover, some proposals directly associated with microgrid protection could be found, such as [11]–[15]. Regarding new solutions and characteristics for microgrid protection, it is important to highlight that their hardware assessment is utterly imperative to a further safe and reliable operation in the field. This concern was also pointed out by the literature review conducted in [10], where it was concluded that only few investigations aim to perform experimental studies and validate the efficiency of this new kind of protection.

Considering the need for new solutions for protecting microgrids (as discussed in [6]), and to conduct experimental investigations concerning non-standard characteristics (as discussed in [10]), this paper presents a hardware-in-the-loop (HIL) testbed for microgrid protection considering non-standard curves. The most recent proposition, to the best of our knowledge, of a non-standard characteristic

This work was supported by the São Paulo Research Foundation (FAPESP) [Grant Number 2017/16742-7 and 2015/21167-6] and Coordenação de Aperfeiçoamento de Pessoal de Nível Superior – Brazil (CAPES) [Finance Code 001]. P. H. A. Barra, V. A. Lacerda, and D. V. Coury are affiliated with the Department of Electrical and Computer Engineering, São Carlos School of Engineering, University of São Paulo, SP, Brazil (e-mail of corresponding author: pedrobarra@usp.br). R. A. S. Fernandes is affiliated with the Department of Electrical Engineering, Federal University of São Carlos, SP, Brazil.

Paper submitted to the International Conference on Power Systems Transients (IPST2021) in Belo Horizonte, Brazil June 6-10, 2021.

was proposed by [15]. Thus, this characteristic is used in the present paper for testing purposes. To do this, four Texas Instruments C2000 Delfino F28379D microcontroller unit (MCU) Launchpad tools [16] were used to represent the microgrid's digital relays. The real-time digital simulator (RTDS) [17] was used to conduct real-time experiments, injecting the analog signals into the MCUs and receiving the digital signals (trips) from them, closing the loop. A test microgrid was simulated in PSCAD for generating the tests presented in this paper. Two MCUs were embedded with a standard characteristic curve to provide a performance reference for the non-standard protection characteristic. Thus, this paper also provides a hardware-performance comparison between the standard overcurrent protection and the non-standard one. The novelty of this paper is the development of a dedicated HIL testbed to test non-standard curves and other innovations, which cannot be easily done in a testbed previously designed to generic overcurrent relays. Thus, the main contributions for the microgrid protection area are highlighted below:

- Design of a dedicated HIL testbed focused on microgrid protection.
- Hardware-based evaluation of non-standard characteristics. As highlighted in [10], there is a limited number of experimental investigations related to the non-standard characteristics reported in the literature.
- The conducted investigations show a hardware-based comparison between standard and non-standard characteristics for microgrid protection, showing evidence that the non-standard one is promising for this task.
- The presented HIL testbed could be useful for further investigations considering the entire microgrid protection and non-standard characteristic propositions and strategies.
- Useful guidelines are provided for hardware implementation of these characteristics.

The remainder of this paper is organized as follows. Section II briefly discusses the challenges in microgrid protection and the non-standard protection curves. Section III presents the specific details associated with the proposed HIL testbed for microgrid protection. Section IV shows the real-time experiments considering faulty situations in a test microgrid. Section V presents the conclusions of this paper.

II. Challenges in Microgrid Protection and Non-standard Protection Curves

In the literature, some studies emphasized the difficulties found in microgrid protection, which are mainly associated with the changes in fault currents and the flexible operation of microgrids [6]. Therefore, conventional protection schemes based on standard overcurrent protection and fixed adjustments may be ineffective for some microgrid's operating situations. One of the standard overcurrent characteristics, provided by the IEEE C37.112-2018 standard [18], is shown in (1):

$$t = \left(\frac{k_1}{{M_I}^{k_2} - k_3} + k_4 \right) \times TMS, \tag{1}$$

where t, M_I, and TMS are the relay operating time, multiple of pickup current (I_f/I_p), and time multiplier setting, respectively. k_1, k_2, k_3, and k_4 are the coefficients of the standard overcurrent curve. Although this standard curve considering adaptive settings has been commonly researched in the protection of distribution networks with distributed generators and microgrids, note that the relay's operating time substantially depends on the fault current seen by the protective device. Thus, due to the low fault current contribution of inverter-based generators into the microgrids, the protection scheme's correct operation can be challenging, leading to relatively high operating times. This challenge is higher when the microgrid operates in an islanded manner since the main grid does not feed the faults.

Non-standard curves appear as a possible alternative for standard overcurrent curves, especially in this low-fault-current scenario. Several proposals can be found in [10], where some authors propose hybrid tripping characteristics using both current and voltage measurements. It is an interesting approach because the relay uses the existing voltage transformer already used for directional protection. An example of a non-standard characteristic, proposed by [15], is shown in (2):

$$t = \left(\frac{k_1}{{M_I}^{k_2} - k_3} + k_4 \right) \times \left(\frac{k_5}{1 - {M_V}^{k_6}} + k_7 \right) \times TMS, \tag{2}$$

where M_V is the multiple of pickup voltage (V_f/V_p), and k_5, k_6, and k_7 are the coefficients of the non-standard hybrid tripping characteristic. Notably, different from (1), the non-standard characteristic described in (2) makes the tripping time depend not only on the measured current, but also on the measured voltage at the protective device during faults. Therefore, even if the fault current is not high (mainly in islanded operating mode), as the voltage drops substantially during the faults, the tripping time tends to be lower in these non-standard schemes.

Figure 1 depicts the operation of the standard characteristic and the non-standard one, where their differences can be observed. Coefficients k_1, k_2, k_3, k_4, k_5, k_6, and k_7 used for this illustration were, respectively, 0.0515, 0.02, 1.0, 0.114, 0.03, 0.5, and 0.0. The TMS value was 0.10 for both. In Fig. 1, it can be observed that the non-standard characteristic may have different tripping times for the same current because it depends on the voltage during the fault. Alternatively, the standard characteristic is independent of the voltage during the fault. The multi-variable (voltage and current) characteristic can be desired in microgrid protection, as the fault current values are not high in the islanded mode, but the voltage drops considerably.

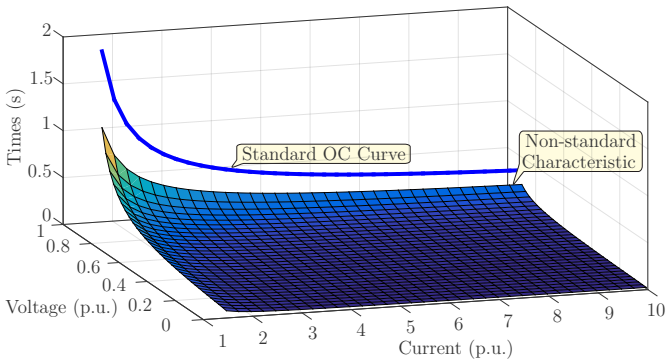

Fig. 1. Standard OC curve and the non-standard OCUV characteristic.

A hypothetical example is used to highlight the differences between these characteristics. Fig. 2 depicts the three-phase currents and voltages measured at the terminals of a type IV wind turbine generator in a microgrid for a specific fault situation, where the values are presented in p.u. The fault inception occurs at $t = 7.0$ s, where it can be seen that the wind turbine generator fault current is about 1.42 p.u. During this fault, the voltage drops from 1.0 to 0.2 p.u. As depicted in Fig. 3, the standard overcurrent protection presents difficulties in enabling this fault isolation because the fault current is near the pickup value, leading to a tripping time of 2.330 s. Moreover, the non-standard characteristic presents a tripping time of 0.121 s due to the considerable voltage drop during the fault. Based on this simple example, it is evident that non-standard characteristics may be useful and desired in protecting the entire microgrid. It is important to clarify that the coordination problem for this non-standard characteristic (explored in-depth by [15]) is similar to that seen for the standard curves and was not the focus of this work. It is also noteworthy that the combination of current and voltage in (2) allows coordination between primary and backup operations. This coordination could not be achieved when using just the undervoltage function for the entire microgrid protection scheme. Thus, the voltage plays an important role in (2), but the current is essential to allow possible coordination among the relays.

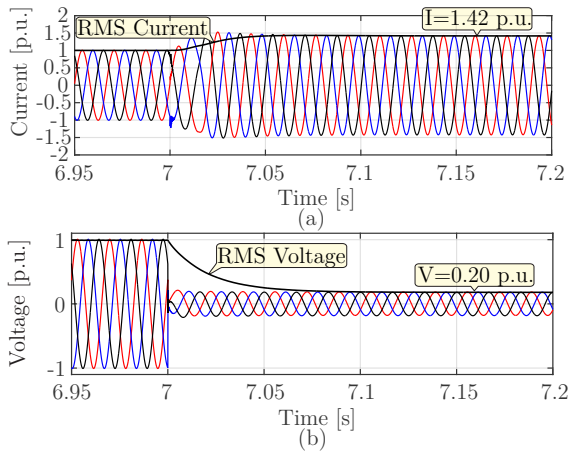

Fig. 2. A fault response of a type IV WTG. a) Current from WTG; b) Measured voltage.

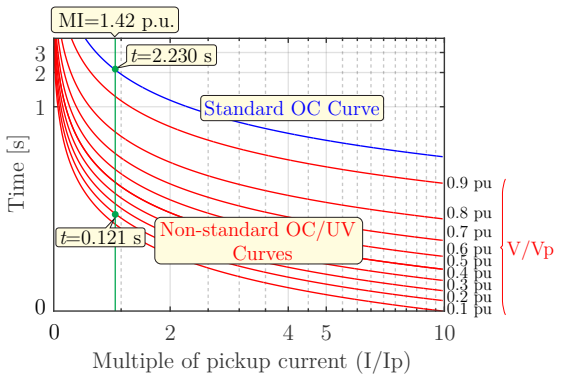

Fig. 3. Practical illustration of tripping characteristics.

III. Proposed HIL Testbed for Microgrid Protection

This section presents information concerning the proposed HIL testbed for microgrid protection. Moreover, information about the experimental setup and the microgrid used for testing is provided.

A. Experimental Setup

The experimental setup used for testing the microgrid protection is depicted in Fig. 4. In this figure, note that computer 1 ran the RSCAD software, which reproduced the voltage and current signals acquired by the protective devices in the microgrid. These signals loaded in the RTDS were obtained from PSCAD, where a test microgrid was modeled. The RTDS converted these signals to analog voltage signals between 0 and 3 V. After that, signals flowed throughout passive anti-aliasing filters. The first-order filters' parameters were $R = 680\ \Omega$ and $C = 680$ nF, with a cut-off frequency of 360 Hz. After filtering, the current and voltage signals were injected into the MCUs. Finally, the digital signals (protection trips) from each MCU were injected into RTDS, closing the loop as shown in Fig. 4.

As mentioned before, the MCUs used in this paper for representing the digital relays and embedding the protection curves were the C2000 Delfino F28379D MCU Launchpad, designed by Texas Instruments [16]. It is a simple and low-cost development board and has four independent 12-bit/16-bit analog-to-digital (ADC) converter modules. Some recent articles can be found in the literature using this MCU to validate protection algorithms and other experimental purposes, for example, [19], [20].

The constructed experimental setup had four MCUs, making it possible to test different fault situations in a microgrid considering primary and backup protection. For each MCU, six 12-bit ADC modules were used for sampling the three-phase voltage and current signals, with a resolution of 4,096 levels. The experiments considered a sampling rate of 32 samples/cycle. Since there was a need to scale all the signals to a range of 0–3 V, the following scales were used – i) for the two forward relays: 3.7 kA represented 3 V, -3.7 kA represented 0 V, 16.5 kV represented 3 V, and -16.5 kV represented 0 V; ii) for the two backward relays: 160 A represented 3 V, -160 A represented 0 V, 16.5 kV represented

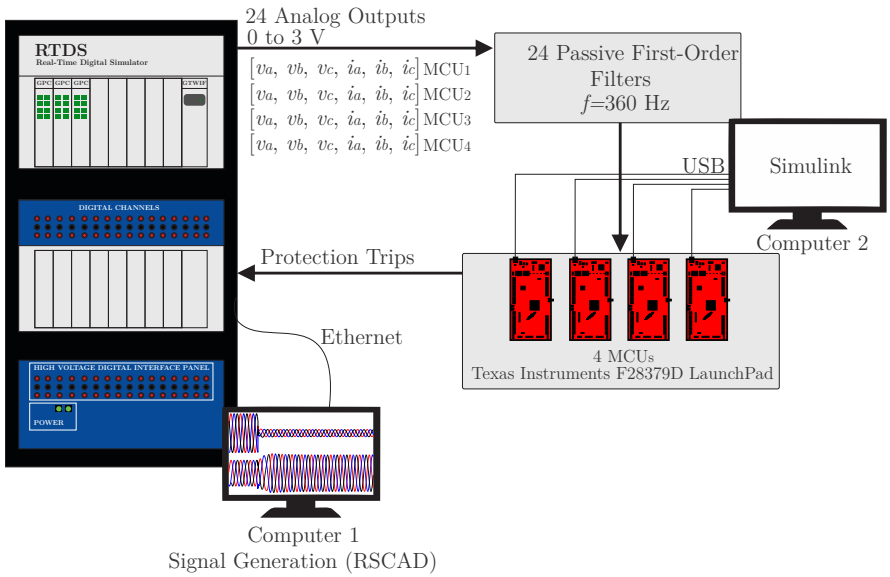

Fig. 4. Experimental setup used for testings.

3 V, and -16.5 kV represented 0 V. It is worth mentioning that this differentiation in scaling was needed due to the major difference between the fault current depending on the fault direction. As a result, a total of 4 digital signals and 24 analog signals were used in the experimental tests. Fig. 5 illustrates the final practical assembly used.

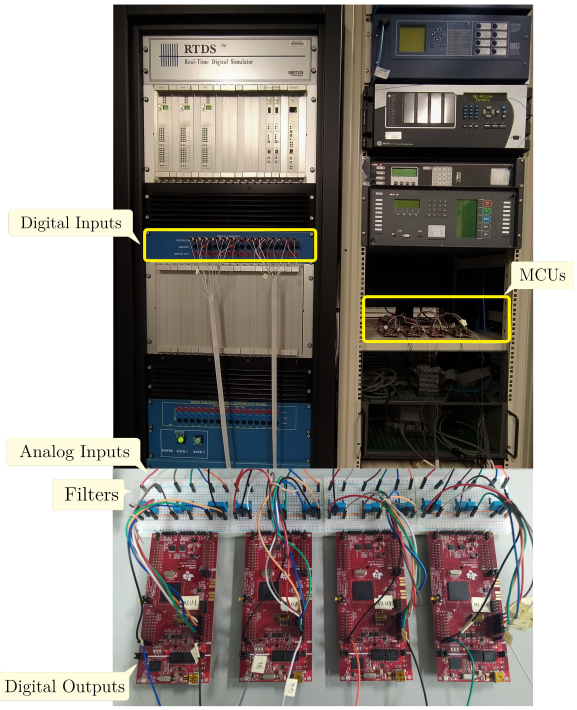

Fig. 5. Practical assembly used for microgrid protection testing.

B. Embedding standard and non-standard curves into MCUs

The standard procedure for embedding algorithms in the F28379D Launchpad is to use C functions with hardware libraries. However, an automatic code generator was adopted to embed the algorithms in the MCUs using the Simulink/Matlab and the Simulink Coder (formerly Real-Time Workshop) [21] based on the rapid-prototyping concept. Thus, considering the F28379D Launchpad characteristics, blocks were used to construct the protection logic associated with the standard and non-standard curves. The fundamental frequency component of the signals was extracted using the Discrete Fourier Transform.

C. Microgrid used for testing

The microgrid used to verify the efficiency of the HIL testbed was modeled in PSCAD. This microgrid was based on the medium-voltage CIGRE benchmark for integrating renewable and distributed energy resources [22] and is depicted in Fig. 6. The nominal voltage of this microgrid was 20 kV with a load of 4.32 MW and 1.43 MVAr. Additional parameters of this network can be found in [22]. Some distributed energy resources were located in this microgrid: a synchronous-based distributed generator (5 MVA) at node 5 and a type IV wind turbine generator (2 MW) integrated with a battery energy storage system (1 MW) at node 8. In Fig. 6, note that the microgrid's boundary limits were well defined, and islanding occurred when the point of common coupling (PCC) with the main grid opened. The 5 MVA synchronous generator represented a conventional dispatchable source, operating in P-Q control mode for the grid-connected operating mode and f-V control mode for the islanded operating mode [23]. As mentioned in [24], grid-connected converters can provide fault currents of 1.1–1.5 p.u. of their nominal currents. Some studies can be found pointing out that these contributions can reach 2 p.u. Thus, a fault current limitation of 1.5 p.u. was considered in the wind turbine generator control. In this microgrid, the battery energy storage system was used for wind power smoothing purposes [25], i.e., it absorbed/supplied power when necessary.

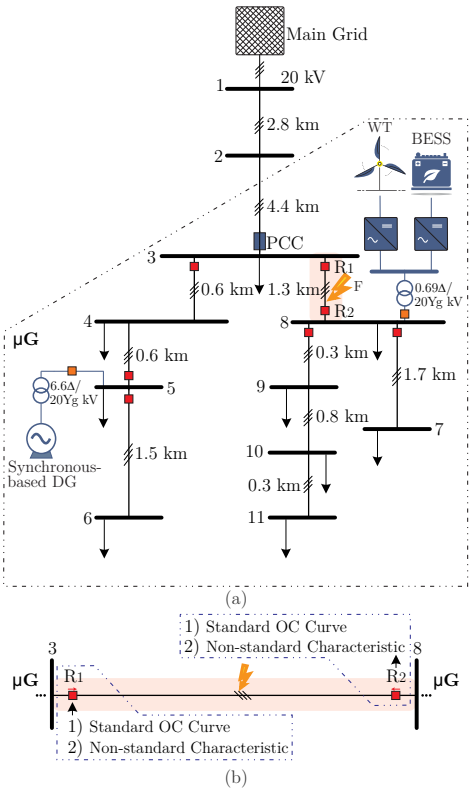

Fig. 6. Microgrid used for testing. a) Microgrid; b) Location of relays used for testing the non-standard characteristic.

Regarding the protection of this microgrid, it can be observed in Fig. 6 that there were some protective devices (directional overcurrent relays) with the microgrid feeders. Particularly, in this paper, the analyses were focused on the digital relays R_1 and R_2. As indicated in Fig. 6b, the purpose was to test these relays when embedded with standard and non-standard protection curves. The adjustments of relays R_1 and R_2 are presented in Table I, where it can be observed that the same values were used for relay constants k_1, k_2, k_3, and k_4. Moreover, the TMS value was also the same for the standard and non-standard curves, allowing a comparison between them. The pickup values were judiciously chosen as follows. The voltage setting values were selected as 70% of the rated voltage (for R_1 and R_2). Moreover, the current setting values were 93 A and 24 A for R_1 and R_2, respectively.

TABLE I
ADJUSTMENTS OF RELAYS R_1 AND R_2 CONSIDERING THE STANDARD (OC) AND NON-STANDARD (OCUV) CURVES

Relay	**Curve**	k_1	k_2	k_3	k_4	k_5	k_6	k_7	TMS
R_1	OC	0.0515	0.020	1.0	0.114	–	–	–	0.38
	OCUV	0.0515	0.020	1.0	0.114	0.03	0.5	0	0.38
R_2	OC	0.0515	0.020	1.0	0.114	–	–	–	0.15
	OCUV	0.0515	0.020	1.0	0.114	0.03	0.5	0	0.15

IV. REAL-TIME EXPERIMENTS

Real-time experiments of the microgrid protection are presented. For all the tests, the voltage and current signals measured from relays R_1 an R_2 are shown. The digital signals from RTDS sent by the MCUs representing the trips from relays are also demonstrated. For each test, the trips from the standard protection curve – R1(OC) and R2(OC) –, as well as the trips from the non-standard protection curve – R1(OCUV) and R2(OCUV) – are displayed.

A. Tests

The first test was a 10 Ω CG fault (phase C to ground fault) considering the islanded operating mode of the microgrid. The results of this scenario are presented in Fig. 7. It can be noticed that, as the current measured by R_2 was relatively low (because of the low contribution current from the wind turbine generator), the resulting operating time of R_2 when considering the standard overcurrent curve was higher (712.2 ms). Alternatively, even with a moderate drop in the voltage during this fault, the non-standard protection was 25 times faster (27.7 ms).

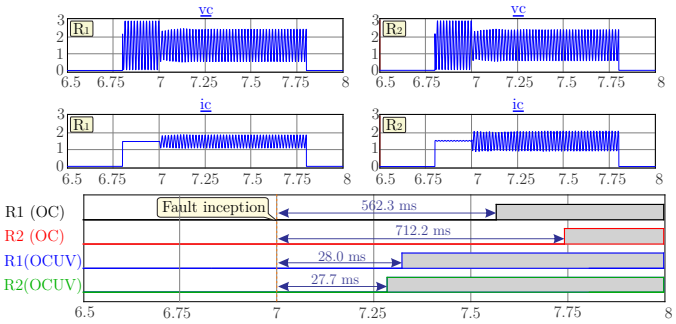

Fig. 7. Real-time test I: a 10 Ω CG fault with islanded microgrid. Currents and voltages measured from R1 and R2, and the trips are depicted.

In the second test, similar behavior was verified. It was a 5 Ω CG fault, however, with a grid-connected microgrid. The results of this test are presented in Fig. 8. Once more, due to the low current in the reverse direction, the tripping time of R_2 was considerably high (709.2 ms). In the forward direction, the tripping time was 426.4 ms. On the other hand, considering non-standard curve protection, the tripping times were 25.8 and 21.5 ms for the forward and backward relays.

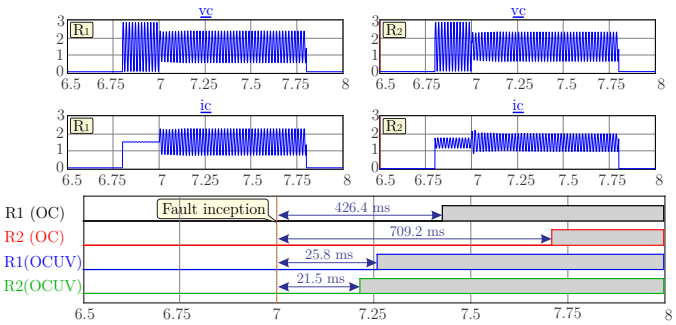

Fig. 8. Real-time test II: a 5 Ω CG fault with grid-connected microgrid.

The protection performance for a 5 Ω ABCG fault considering the islanded microgrid is depicted in Fig. 9. Due to the voltage drop, the non-standard protection (OCUV) was also faster. It should be mentioned that for solid faults, the

voltage drop was more accentuated. This is the case reported in Fig. 10 when a solid ABCG fault with the grid-connected microgrid was analyzed. In this situation, the non-standard protection presented a very fast tripping time.

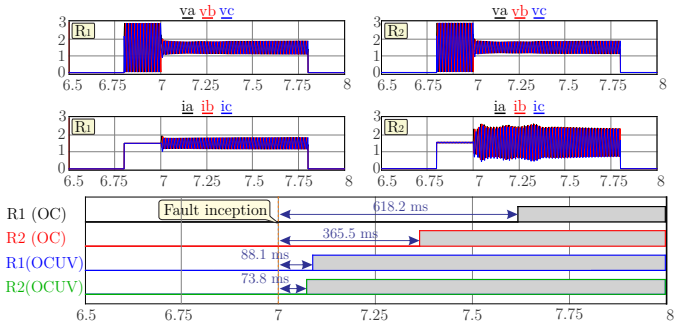

Fig. 9. Real-time test III: a 5 Ω ABCG fault with islanded microgrid.

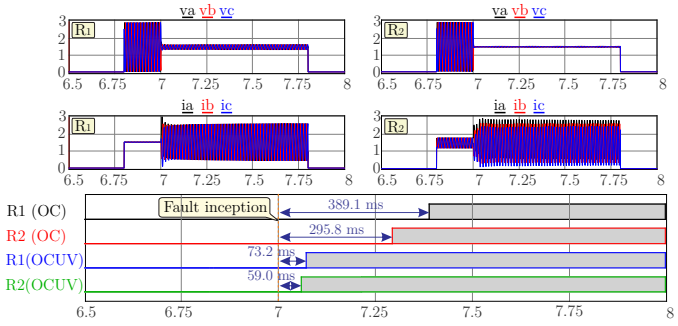

Fig. 10. Real-time test IV: a solid ABCG fault with grid-connected microgrid.

When a solid ABCG fault occurred with the islanded microgrid (Fig. 11), the fault current was less than that measured in the grid-connected microgrid (Fig. 10). In this situation, while the standard overcurrent protection presented a high tripping time, the non-standard protection presented a fast tripping time due to the considerable voltage drop. It is worth highlighting that as protective devices should present a coordinated operation for the whole microgrid protection, the presented performance of non-standard protection curves may be helpful. This is because it performed adequately for different scenarios with a fast response.

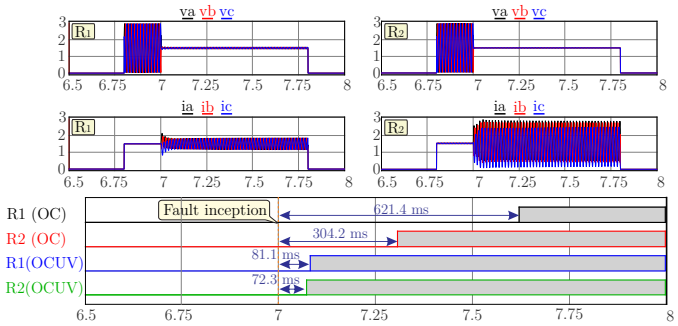

Fig. 11. Real-time test V: a solid ABCG fault with islanded microgrid.

B. Hardware Implementation Accuracy

In order to analyze the accuracy of the hardware implementation presented in this paper, a comparison between the tripping times achieved from the hardware implementation and the computational simulations was performed. Table II shows the obtained differences for the five tests presented in this paper, considering tripping times of the standard and non-standard curves. Fig. 12 graphically depicts this comparison, where it can be concluded that performance between hardware implementation and simulation results was very similar.

TABLE II
COMPARISON BETWEEN RESULTS OBTAINED FROM THE HARDWARE IMPLEMENTATION AND THE COMPUTATIONAL SIMULATIONS (SECONDS)

Test	Relay	Software	Hardware	Difference
I	R1 (OC)	0,554	0,562	0,008
	R2 (OC)	0,601	0,712	0,111
	R1 (OCUV)	0,257	0,280	0,023
	R2 (OCUV)	0,221	0,277	0,057
II	R1 (OC)	0,411	0,426	0,016
	R2 (OC)	0,603	0,709	0,106
	R1 (OCUV)	0,222	0,258	0,036
	R2 (OCUV)	0,201	0,215	0,014
III	R1 (OC)	0,596	0,618	0,022
	R2 (OC)	0,296	0,366	0,069
	R1 (OCUV)	0,056	0,088	0,032
	R2 (OCUV)	0,056	0,074	0,018
IV	R1 (OC)	0,370	0,389	0,019
	R2 (OC)	0,268	0,296	0,028
	R1 (OCUV)	0,057	0,073	0,017
	R2 (OCUV)	0,055	0,059	0,004
V	R1 (OC)	0,590	0,621	0,031
	R2 (OC)	0,277	0,304	0,028
	R1 (OCUV)	0,055	0,081	0,027
	R2 (OCUV)	0,055	0,072	0,018

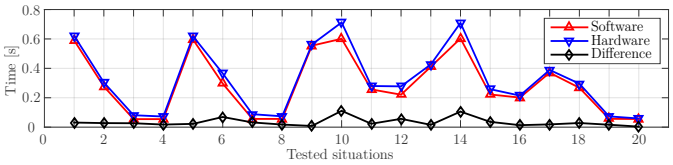

Fig. 12. Obtained tripping times for all tested situations: hardware and software comparison.

V. Conclusions

This paper presented an HIL testbed for microgrid protection considering non-standard curves. Standard and non-standard protection curves were embedded in four Texas Instruments C2000 Delfino F28379D MCU Launchpad tools, enabling us to compare them. It is important to clarify that real-time experiments, such as the ones presented here, are imperative for safely implementing real-world non-standard curves. A comparison between the standard and non-standard curves was shown using hardware results, where the non-standard one proved to be more advantageous. Moreover, the findings showed that the hardware implementation was successful as the simulation and hardware results were similar. The presented validation and guidelines concerning hardware

implementation should be useful for future research related to microgrid protection. Future work should focus on the use of this dedicated HIL testbed to study the microgrid protection with non-standard curves and other innovations, considering adaptive protection schemes with different relay settings.

REFERENCES

[1] Y. Yang, S. Bremner, C. Menictas, and M. Kay, "Battery energy storage system size determination in renewable energy systems: A review," *Renewable and Sustainable Energy Reviews*, vol. 91, pp. 109 – 125, 2018.

[2] N. Hatziargyriou, H. Asano, R. Iravani, and C. Marnay, "Microgrids," *IEEE Power and Energy Magazine*, vol. 5, no. 4, pp. 78–94, 2007.

[3] H. Haddadian and R. Noroozian, "Optimal operation of active distribution systems based on microgrid structure," *Renewable Energy*, vol. 104, pp. 197 – 210, 2017.

[4] S. Chandak and P. K. Rout, "The implementation framework of a microgrid: A review," *International Journal of Energy Research*, vol. 45, no. 3, pp. 3523–3547, 2021.

[5] M. A. Hossain, H. R. Pota, M. J. Hossain, and F. Blaabjerg, "Evolution of microgrids with converter-interfaced generations: Challenges and opportunities," *International Journal of Electrical Power Energy Systems*, vol. 109, pp. 160 – 186, 2019.

[6] P. H. A. Barra, D. V. Coury, and R. A. S. Fernandes, "A survey on adaptive protection of microgrids and distribution systems with distributed generators," *Renewable and Sustainable Energy Reviews*, vol. 118, p. 109524, 2020.

[7] M. Ghalei Monfared Zanjani, K. Mazlumi, and I. Kamwa, "Application of μPMUs for adaptive protection of overcurrent relays in microgrids," *IET Generation, Transmission & Distribution*, vol. 12, no. 18, pp. 4061–4068, 2018.

[8] T. S. S. Senarathna and K. T. M. U. Hemapala, "Optimized adaptive overcurrent protection using hybridized nature-inspired algorithm and clustering in microgrids," *Energies*, vol. 13, no. 13, 2020.

[9] S. A. Hosseini, S. H. H. Sadeghi, and A. Nasiri, "Decentralized adaptive protection coordination based on agents social activities for microgrids with topological and operational uncertainties," *IEEE Transactions on Industry Applications*, vol. 57, no. 1, pp. 702–713, 2021.

[10] H. C. Kiliçkiran, İbrahim Şengör, H. Akdemir, B. Kekezoğlu, O. Erdinç, and N. G. Paterakis, "Power system protection with digital overcurrent relays: A review of non-standard characteristics," *Electric Power Systems Research*, vol. 164, pp. 89 – 102, 2018.

[11] N. El-Naily, S. M. Saad, T. Hussein, and F. A. Mohamed, "A novel constraint and non-standard characteristics for optimal over-current relays coordination to enhance microgrid protection scheme," *IET Generation, Transmission & Distribution*, vol. 13, no. 6, pp. 780–793, 2019.

[12] A. Darabi, M. Bagheri, and G. B. Gharehpetian, "Highly sensitive microgrid protection using overcurrent relays with a novel relay characteristic," *IET Renewable Power Generation*, vol. 14, no. 7, pp. 1201–1209, 2020.

[13] S. D. Saldarriaga-Zuluaga, J. M. López-Lezama, and N. Muñoz-Galeano, "Optimal coordination of overcurrent relays in microgrids considering a non-standard characteristic," *Energies*, vol. 13, no. 4, 2020.

[14] L. Ji, Z. Cao, Q. Hong, X. Chang, Y. Fu, J. Shi, Y. Mi, and Z. Li, "An improved inverse-time over-current protection method for a microgrid with optimized acceleration and coordination," *Energies*, vol. 13, no. 21, 2020.

[15] S. Chakraborty and S. Das, "Communication-less protection scheme for ac microgrids using hybrid tripping characteristic," *Electric Power Systems Research*, vol. 187, p. 106453, 2020.

[16] Texas Instruments, *TMS320F2837xD Dual-Core Microcontrollers Datasheet (Rev. M)*, (accessed November 11, 2020), available at http://ti.com/lit/pdf/SPRS880M.

[17] RTDS Technologies, (accessed November 11, 2020), available at https://www.rtds.com/about-rtds-technologies/.

[18] IEEE, "IEEE standard for inverse-time characteristics equations for overcurrent relays," *IEEE Std C37.112-2018 (Revision of IEEE Std C37.112-1996)*, pp. 1–25, 2019.

[19] V. A. Lacerda, R. M. Monaro, D. Campos-Gaona, D. V. Coury, and O. Anaya-Lara, "Distance protection algorithm for multiterminal HVDC systems using the Hilbert-Huang transform," *IET Generation, Transmission & Distribution*, vol. 14, no. 15, pp. 3022–3032, 2020.

[20] R. F. Bastos, F. B. Silva, C. R. Aguiar, G. Fuzato, and R. Q. Machado, "Low-cost hardware-in-the-loop for real-time simulation of electric machines and electric drive," *IET Electric Power Applications*, vol. 14, no. 9, pp. 1679–1685, 2020.

[21] Simulink Coder, (accessed November 14, 2020), available at https://www.mathworks.com/products/simulink-coder.html.

[22] CIGRE Working Group C6-04, *Technical Brochure 575: Benchmark Systems for Network Integration of Renewable and Distributed Energy Resources*. CIGRE, 2014.

[23] T. S. Menezes, R. A. Fernandes, and D. V. Coury, "Intelligent islanding detection with grid topology adaptation and minimum non-detection zone," *Electric Power Systems Research*, vol. 187, p. 106470, 2020.

[24] A. A. Memon and K. Kauhaniemi, "An adaptive protection for radial AC microgrid using IEC 61850 communication standard: Algorithm proposal using offline simulations," *Energies*, vol. 13, p. 5316, 2020.

[25] P. H. A. Barra, W. C. de Carvalho, T. S. Menezes, R. A. S. Fernandes, and D. V. Coury, "A review on wind power smoothing using high-power energy storage systems," *Renewable and Sustainable Energy Reviews*, vol. 137, p. 110455, 2021.